Sensors and Actuators A 218 (2014) 167–178

Contents lists available at ScienceDirect

Sensors and Actuators A: Physical

journal homepage: www.elsevier.com/locate/sna

Theoretical and experimental investigations of the temperature and thermal deformation of a giant magnetostrictive actuator

Yuchuan Zhu*, Liang Ji

College of Mechanical and Electrical Engineering, Nanjing University of Aeronautics and Astronautics, Nanjing 210016, China

ARTICLE INFO

Article history:
Received 16 March 2014
Received in revised form 16 July 2014
Accepted 19 July 2014
Available online 28 July 2014

Keywords:
Giant magnetostrictive material
Actuator
Heat transfer
Finite element method
Temperature

ABSTRACT

Giant magnetostrictive actuators (GMAs) have received considerable attention in recent years and are becoming increasingly important in the exploitation of new type electromechanical devices. The performance of giant magnetostrictive actuator (GMA) is generally determined by the precision of the GMA output displacement; however, the heat-induced displacement of a GMA is the principal element influencing the precision of the GMA output displacement. In this paper, a precise GMA with a heat-induced displacement suppression system is developed; the heat-induced displacement control mechanism consists of a temperature control module and a thermal displacement compensation module. Based on the heat-transfer rules, a GMA heat-transfer mathematical model and a GMM rod heat-induced displacement model are built; next, the mathematical models of GMA heat-transfer are solved and the temperature distribution, the heat-induced displacement, and the heat transfer rate of GMA are completely obtained. Finally, a test system for a GMA heat-induced displacement suppression system is implemented, and an experimental study of the system is performed. The results of the GMA heat-induced displacement by experimental research basically coincide with the results of the GMA heat-transfer mathematical model, that is, the GMA temperatures are controlled to below 35 °C and the GMA heat-induced displacement remains within a small range under an input current of 1 A for a period of continuous operation of 80 min. The system observably improved the precision of the GMA output displacement; as a result, the research results provided a basis for a precise micro-displacement GMA.

1. Introduction

Giant magnetostrictive materials (GMMs) dubbed Terfenol-D enabled the development of a totally new class of electromechanical devices with higher energy density, faster response, and better precision than previously possible [8,14,15,18,19,21,31,32]; such devices can be applied for use in sound and vibration sensors [22], sonar systems [13], active vibration control systems [32], micro-motional control [20], magnetostrictive motors [10,20], hydraulics [5,12,23,24], and sensors [6]. Magnetostrictive devices are fairly robust as far as wear and tear are concerned, which exhibit their potential for replacing traditional piezoelectric devices.

Giant magnetostrictive actuators (GMAs) are one of the most exciting new actuator technologies available today, which have created new design options for mechanical and electrical engineers alike; however, GMAs are complex structures requiring a careful design, with the performance of a GMA determined directly by the precision of the GMA output displacement, which is dependent on the coupling deformation displacement due to magnetostrictive deformation and thermal deformation. Therefore, determining how to decouple, inhibit, and control the thermal deformation displacement are the difficult points and key technologies required for improving the precision of the GMA output displacement.

For high-power GMAs, forced cooling measures or constant temperature control methods are common approaches to achieve a GMA high-precision output displacement, which uses water circulation between the GMM rod and the exciting coil to remove the heat generated by the GMM rod and the exciting coil and, accordingly, to ensure the GMM rod temperature accurately remains within a certain small range. For example, Jia [7] cooled the GMM rod using a spiral water cooling tube outside of the GMM rod. Lu et al. [16] adopted the internal and external double water cooling mechanism to further reduce the thermal displacement to 0.02 μm. Wang [24] developed a type of the real-time compensation system based on a thermal compensation pipe, which uses hydraulic oil as a cooling medium to cool the GMM rod; they performed experiments both in summer and winter, and the experiment results indicated that the GMM rod temperature rise is rapid at the

* Corresponding author. Tel.: +86 18951674995; fax: +86 2584891501.
E-mail address: meeyczhu@nuaa.edu.cn (Y. Zhu).

http://dx.doi.org/10.1016/j.sna.2014.07.017
0924-4247/

beginning, but after the temperature rose to a certain value, it tended to reach equilibrium, and the system achieved a relatively satisfactory thermal displacement control effect. Furthermore, the phase change temperature control method [4], which keeps the GMM rod temperature constant by using some phase change materials to absorb or release a large amount of latent heat in the process of phase change to enable the GMM rod temperature remains nearly unchanged. Anjianappa applied this method to attempt to maintain the temperature of the GMM rod in a certain range; however, because of the limitation of the heat absorption capacity of the phase change materials, the GMM rod temperature can only remain constant over a short time. The subsequent improvement method is called the combined temperature control method, which uses both water or semiconductor material and phase change materials to cool the GMM rod, in other words, the water on the outside of the coil is used to prevent thermal deformation of the shell, and the phase change materials on the inside of the coil is used to inhibit thermal deformation of the GMM rod. Wu performed an experiment [26] that indicated if no cooling measures were taken, the temperature of the GMM rod would exceed 100 °C in the fourth hour when the GMA begin working, but by using the combined temperature control measures, the GMM rod temperature can be maintained to within 45 ± 0.5 °C, during which time, the output displacement of the GMM rod caused by the temperature fluctuation is not more than 0.1 μm. Semiconductor refrigeration is a method that involves the contact surfaces being coated with thermal silicone grease to increase the coefficient of thermal conductivity [9] of the surface in contact with several semiconductor thermopiles that are installed on both ends of a coil bobbin to enable cooling water to flow past the hot end of thermopile, which can strengthen the radiating effect and ensure that there is a higher cooling efficiency. Kwak [27] used a compressed air to cool the GMM rod; through a finite element analysis and experiment research, they concluded that a cooling air temperature of 18 °C and an air velocity of 2.8 m/s represent the optimal cooling conditions.

For a small power GMAs, the passive thermal deformation compensation method often is used, mainly including the software compensation method, the thermal expansion offset method, and the flexible support compensation method. The software compensation method is simple to use [29]. In the GMA using the software compensation method, the temperature control component is installed on the GMM rod, and the controller is used to compensate the heat-induced displacement of GMM rod; the GMA does not require additional hardware system, but its heat-induced displacement control precision is not high. The thermal expansion offset method [28] in a precision GMA with 20 μm stroke and a 1 mm × 1 mm × 20 mm GMM rod is placed on the stainless steel coil bobbin, which has the same thermal expansion coefficient as the GMM rod. The external surface of the GMA uses an invar alloy that has a very low thermal expansion rate, so the GMM rod thermal deformation is offset by the stainless steel coil bobbin thermal elongation. The basic idea of flexible support compensation is to utilize the GMA coil bobbin thermal expansion to drive a flexible hinge mechanism, which adjusts in real time the position of the GMM rod bottom support point, thus inhibiting the GMA heat-induced displacement output during GMA operation. Xia [25] designed a flexible hinge compensation device with a supply current of 600 mA; after continuous application of the power supply for 120 min, the thermal deformation of GMA was up to 27 μm without compensation, but the thermal deformation reduced to 7 μm after compensation.

For theoretical research of the GMM rod thermal deformation and the heat-induced displacement control, Zeng et al. [30] used the finite element method (FEM) to calculate the flow field distribution and temperature field distribution of the GMA with a forced cooling system; the cooling system was able to keep the temperature of GMM rod under 70 °C. Stillesjo [3] analyzed the operation of a giant magnetostrictive ultrasonic transducer with a drive current 10 A and frequency of 21 kHz using FEM, and he concluded that the flow rate of the cooling water of 6.8 L/min can keep the temperature of actuator at approximately 80 °C. Li [12] designed a control valve driven by a hollow giant magnetostrictive actuator; in the hollow actuator, the hole is used as a cooling passage to cool the actuator in addition, they studied the change of the GMA temperature as a function of the driven frequency and analyzed the eddy current loss, magnetic hysteresis loss and frequency characteristics of the complex permeability based on the theory of the minimum energy condition and magnetism theory [11]. Anjanappa and Bi [1], Bi [2], Angara [17] proposed a thermal resistance theory that was applied to research on heat transfer and amended the piezomagnetic equation; unfortunately, the deduction of the GMA calculation model on the heat-induced displacement was not performed.

In summary, although there are many compensation structures and control methods to control the GMAs thermal deformation, the effect is not ideal enough to only adopt a single thermal compensation approach, and the existing GMAs thermal displacement control research is mainly in the experimental study phase, with a lack of systematic theoretical research on the GMA heat transmission and heat-induced displacement compensation mechanism. Therefore, it would be of great theoretical and engineering significance to explore the GMA thermal displacement control theory and perform an experimental study of the combination of temperature control and heat-induced displacement compensation.

The thermal displacement control methods above-mentioned are constant temperature control method and passive thermal deformation compensation method, respectively, for the former, the equipment is complex and the real-time temperature control performance is not always satisfactory; for the latter, the coefficient of thermal expansion for the compensating element varies with temperature, so it is difficult to keep the high precision of the thermal deformation compensation in a large temperature range. In this paper, we present a new idea that active and passive control method simultaneously, that is, we reduced the temperature of GMM rod to a small temperature range by means of active control method, obtained a high thermal displacement control precision by use of passive control method, which is easier to achieve in a small temperature range for a GMA. In the present study, a GMA is designed and fabricated with a heat-induced displacement suppression system, which consists of an active GMM rod cooling module and a passive heat-induced displacement compensation module. Next, based on the equivalent thermal resistance theory and the definition of the liquid specific heat capacity, the GMA heat-transfer model at steady-state is established. Subsequently, assuming the coefficient of thermal expansion of the GMM rod is constant, the GMA heat-induced displacement calculation models under both free convection and forced convection are determined. Accordingly, the temperature rise, the heat-transfer rate, and the heat-induced displacement of the GMM rod are calculated according to the present calculation model. Finally, the heat-transfer test system of the GMA is built, and the test results have a good agreement with the theoretical calculation results of the present model, which provides a great contribution to the design and application of a precise GMA.

2. GMA structure and working principle

As Fig. 1 shows, the GMA magnetic circuit is composed of the following components: output shaft, upper end cover, GMM rod, sliding block, preloaded bolt, outer cover, base, etc. By adjusting the preloaded bolt, a appropriate prestress (7 MPa is selected from the

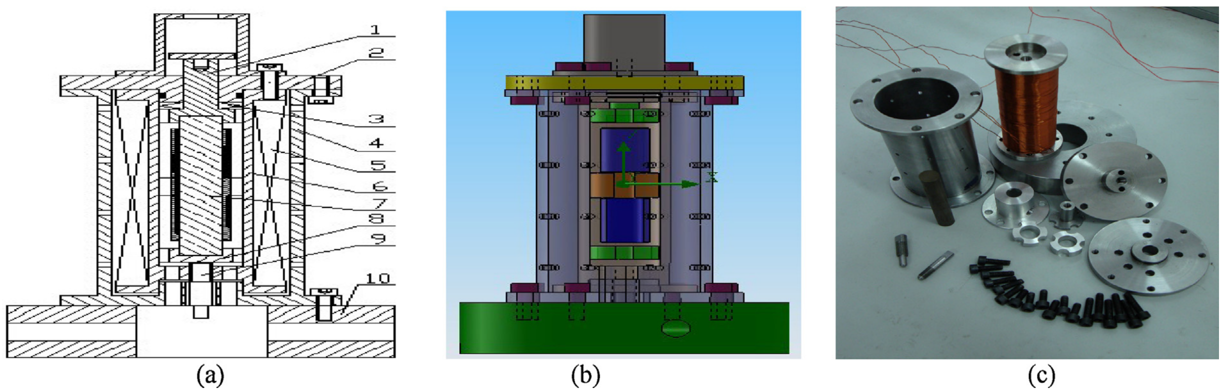

Fig. 1. GMA configuration diagram (1) output shaft; (2) upper end cover; (3) disk spring; (4) outer cover; (5) exciting coil; (6) coil bobbin; (7) GMM rod; (8) sliding block; (9) preloaded bolt; and (10) base.

specification of the manufacturer of GMM rod) is provided for the GMM rod, which make the efficiency and coupling factors of GMA higher than those of the no prestress case. The bias direct current in the exciting coil provides a bias magnetic field for the GMM rod, which enables the GMA operate in the linear region. When the drive current in the exciting coil is switched on, accordingly, the driving magnetic field is established, and the electro-magnetic energy will turn into mechanical energy, thus elongating and shortening the GMM rod, which can make the output shaft move according to the design requirements.

Moreover, an appropriate cooling system must match the overall heat generated during operation. As shown in Fig. 1, the present GMA heat-induced displacement suppression system is composed of an active GMM rod cooling module and a passive GMM rod heat-induced displacement compensation module, and the two modules operate at the same time. The active cooling module is composed of the pump, the liquid (water is selected for the experiment), and the ring runner (between the coil bobbin and the GMM rod), which cools the GMM rod by making the liquid flow past the gap between the coil bobbin and GMM rod; thus, the flowing liquid will take away part of heat generated by the coil when the GMA is operating. The passive heat-induced displacement compensation module is comprised of the coil bobbin, the preloaded bolt, and the flowing liquid. The top of the coil bobbin is connected to the upper end cover of the GMA, and the bottom of the coil bobbin is connected to the preloaded bolt. The coil bobbin and the preloaded bolt can move in the opposite direction of the GMM rod magnetostrictive displacement. When the GMA is operating, the coil bobbin will have thermal expansion downward with a temperature rise due to its upper end being fixed; because the preloaded bolt is connected with the coil bobbin by screw thread, the preloaded bolt will move down as well. As a result, there is a gap between the GMM rod and the bottom sliding block. The GMM rod, meanwhile, also produces a thermal expansion downward for the upward block, which can guarantee that the amounts of their thermal expansions are equal or approximately equal at a certain temperature range, so that the thermal deformation of the GMM rod can be compensated and suppressed.

3. GMA steady-state equivalent thermal resistance model

Because the GMA is an axisymmetric solid of revolution, to simplify the theoretical analysis, it is ignored that all of the screws and other local tiny structures in the GMA; thus, the GMA can be considered as a axisymmetric structure, so, based on the equivalent thermal resistance theory, the GMA heat transfer model is shown in Fig. 2. In Fig. 2, the coil is the heat source, and it has two heat-transfer pathways: first, the heat generated by the coil is conducted to the air through the outer cover; second, the heat is conducted to the GMM rod by the coil bobbin and the liquid. As shown in Fig. 2(a), the GMA steady-state equivalent thermal resistance model under free convection, that is, the liquid between the coil bobbin and the GMM rod is motionless. As shown in Fig. 2(b), the GMA steady-state equivalent thermal resistance model under forced convection, that

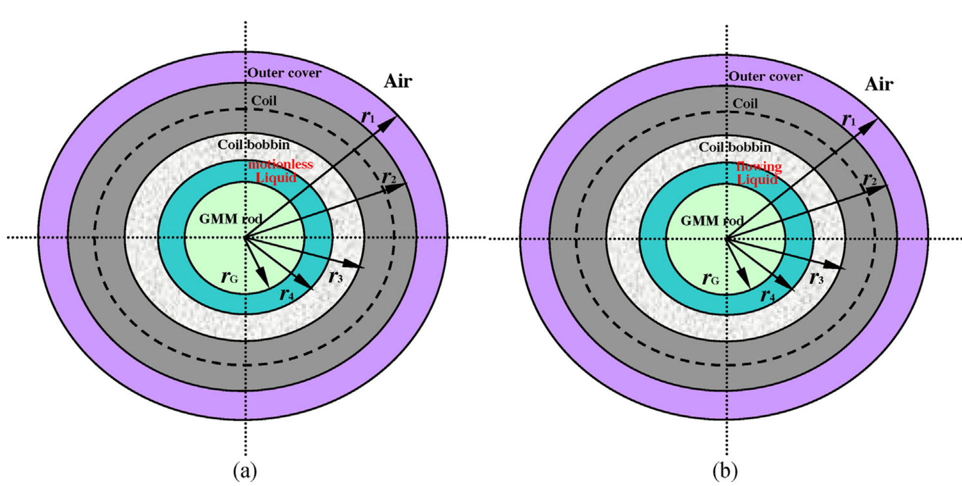

Fig. 2. GMA steady-state equivalent thermal resistance model.

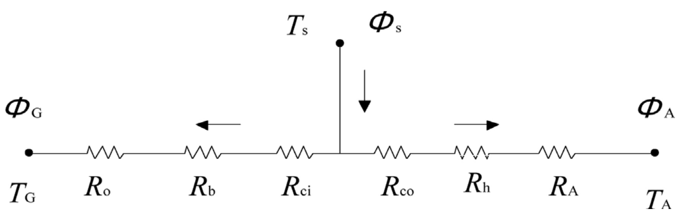

Fig. 3. Equivalent thermal circuit model of the GMA.

is, the liquid between the coil bobbin and the GMM rod is forced to flow by the action of the pump.

Accordingly, the GMA equivalent thermal circuit model is shown in Fig. 3 (Anjanappa et al. [1]; Bi [2]; Angara [17]). Because the coil is a major part of the heat source for the GMA, as the GMA operates in DC or low frequency AC, the quantity of heat generated by the eddy current loss and the hysteresis losses can be ignored; as a result, Φ_s is the *heat transfer rate* produced by the coil under carrying current i and resistance R, Φ_G and Φ_A are the *heat transfer rate* which is conducted to the GMM rod by the coil bobbin and to the air through the outer cover, respectively, T_s is the temperature of the heat source, T_G, T_A is temperature of the GMM rod and the ambient air, respectively, and the expression of Φ_s is:

$$\Phi_s = i^2 R \tag{1}$$

Based on the equivalent thermal resistance model of the GMA, the following formula is obtained

$$\Phi_s = \Phi_G + \Phi_A \tag{2}$$

The configuration of the main component in the GMA is cylindrical, so the heat conduction differential equation in the cylindrical coordinate system is as follows:

$$\rho c \frac{\partial t}{\partial \tau} = \frac{1}{r}\frac{\partial}{\partial r}\left(\lambda r \frac{\partial t}{\partial r}\right) + \frac{1}{r^2}\frac{\partial}{\partial \varphi}\left(\lambda \frac{\partial t}{\partial \varphi}\right) + \frac{\partial}{\partial z}\left(\lambda \frac{\partial t}{\partial z}\right) + \dot{\Phi} \tag{3}$$

It is well-known that there are three distinct modes of heat-transfer: conduction, convection and radiation. In reality, the temperature distribution in the GMM rod is controlled by the combined effects of the above three modes; therefore, it is actually impossible to isolate entirely one mode from the interactions with the other modes. However, for simplicity in the analysis, we consider that the conduction is a dominant factor in the heat flux transfer from the heat source to the outer cover and the coil bobbin, while the convection and the radiation are negligible.

When the GMA operates in DC or low frequency AC, by the analysis of the actual heat-transfer, the mathematical model of GMA heat-transfer at steady state can be simplified to one-dimensional conduction without an inner heat source and the heat conduction coefficient is constant; thus, Eq. (3) can be simplified as:

$$0 = \frac{1}{r}\frac{\partial}{\partial r}\left(\lambda r \frac{\partial t}{\partial r}\right) \tag{4}$$

In a similar way, we consider that a large space free convection is the dominant factor in the heat flux transfer from the outer cover to the ambient air, and finite space compulsory convection is the dominant factor for the heat flux transfer from the coil bobbin to the liquid, while conduction and radiation are negligible.

From the Newton cooling formula

$$\Phi = h_A \Delta t \tag{5}$$

Through simple deduction on the basis of formula (4) and the definition of thermal resistance, the thermal resistance expression can be obtained as follows

$$R_{ci} = \frac{\ln(r_2 + r_3/2r_3)}{2\pi\lambda_c L_b};\ R_{co} = \frac{\ln(2r_2/r_2 + r_3)}{2\pi\lambda_c L_b};\ R_b = \frac{\ln(r_3/r_4)}{2\pi\lambda_b L_b};$$
$$R_h = \frac{\ln(r_1/r_2)}{2\pi\lambda_h L_C} \tag{6}$$

where R_{ci} is the thermal resistance of one half of the coil from the coil center inward, R_{co} is the heat resistance of one half of the coil from the coil center outward, and R_b and R_h are the thermal resistances of the coil bobbin and the outer cover, respectively. L_G is the axial length for the GMM rod. λ_c, λ_b and λ_h are the *thermal conductivities* of the coil, coil bobbin and the outer cover, respectively, L_b and L_C are the lengths of the coil bobbin and the outer cover, respectively.

Through simple deduction on the basis of formula (5) and the thermal resistance definition formula, the thermal resistance expression of R_o and R_A can be obtained as follows:

$$R_o = \frac{1}{2\pi r_3 L_b h_o};\ R_A = \frac{1}{2\pi r_4 L_C h_A} \tag{7}$$

where R_o is the thermal resistance of the heat convection between the inside of the coil bobbin and the liquid, R_A is the thermal resistance of the heat convection between the outer cover and the ambient air, and h_o is *convective heat transfer coefficient* between the coil bobbin and the liquid, with $h_o = h_{o1}$ under free convection and $h_o = h_{o2}$ under forced convection; h_A is *convective heat-transfer coefficient* between the outer cover and the ambient air.

Analogous to Ohm's law in an electrical system, the following equations can be written as:

$$(R_{ci} + R_b + R_o)\Phi_G = T_s - T_G \tag{8}$$

$$(R_{co} + R_h + R_A)\Phi_A = T_s - T_A \tag{9}$$

4. GMA heat-induced displacement calculation model

4.1. GMA heat-transfer model

According to above-mentioned GMA heat-induced displacement control principle, the GMA final heat-induced displacement mainly depends on the preloaded bolt, the GMM rod, the sliding block, the output shaft and the coil bobbin. Based on the model mentioned above, considering the free convection and the forced convection, we determined the calculation models as follows: the temperature rise model and the heat-induced displacement model of the GMM rod and the coil bobbin, and the total heat-induced displacement model for the GMA with and without the heat-induced displacement compensation measures.

According to Fig. 2, the solution of the coil bobbin temperature distribution can be simplified as a one-dimensional heat conduction problem. The outward side of the coil bobbin yields the boundary condition of the second kind, and the inward side of the coil bobbin yields the boundary condition of the third kind; however, the inward temperature of the coil bobbin is time dependent.

After integrating the formula (4) twice, the general solution of the formula (4) can be obtained:

$$t = c_1 \ln r + c_2 \tag{10}$$

where c_1 and c_2 are integration constants determined by the boundary conditions.

For the outward direction of the coil bobbin, the boundary condition is the boundary condition of the second kind, which can be written as follows:

$$\begin{cases} r = r_3 \\ -\lambda_b \dfrac{dt}{dr} = -q_G = -\dfrac{\Phi_G}{2\pi r_3 L_b} \end{cases} \tag{11}$$

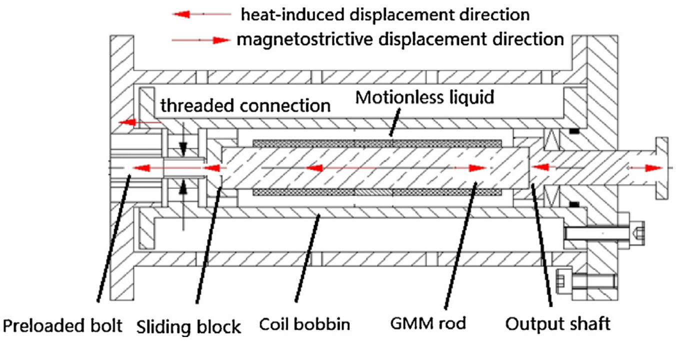

Fig. 4. Thermal compensation of the schematic diagram of the GMA under free convection.

where q_G is the *heat flux* of the outward side of the coil bobbin; minus on the left side of Eq. (11) means that the direction of heat transfer is opposite to the one of temperature rise, and minus on the right side of Eq. (11) means that the direction of heat transfer is opposite with one of cylindrical coordinates.

Substituting (11) into (10) yields

$$\frac{c_1\lambda_b}{r_3} = q_G = \frac{\Phi_G}{2\pi r_3 L_b} \tag{12}$$

For the inward of the coil bobbin, the boundary conditions are as follows:

$$\begin{cases} r = r_4 \\ -\lambda_b \dfrac{dt}{dr} = -h_o(t - t_f) \end{cases} \tag{13}$$

where t_f is the liquid temperature and t_f is time's function under a free convection; minus on the left side of Eq. (13) means that the direction of heat transfer is opposite to the one of the temperature rising, and minus on the right side of Eq. (13) means that direction of the heat transfer is opposite with the one of the cylindrical coordinates.

Substituting (13) into (10) yields

$$\frac{c_1\lambda_b}{r_4} = h_o(c_1 \ln r_4 + c_2 - t_f) \tag{14}$$

Based on simultaneous Eqs. (12) and (14), the coil bobbin temperature distribution T_b can be written as

$$T_b = \frac{\Phi_{G1}}{2\pi\lambda_b L_b}\left(\ln\frac{r}{r_4} + \frac{\lambda_b}{r_4 h_{o1}}\right) + t_f \tag{15}$$

Because the liquid temperature t_f in Eq. (15) is an unknown quantity, we will deduce the expression of t_f under free convection and forced convection. The gap between the coil bobbin and the GMM rod is full of flowing liquid, so, at steady state, the temperature of the liquid t_f is the same as the temperature of the GMM rod; at this time, the heat flow Φ_G generated by coil completely transfers to the liquid.

4.2. GMA heat-induced displacement calculation model under free convection

The thermal compensation schematic diagram of the GMA under free convection is shown in Fig. 4: the GMM rod is fixed on the left end and is compressed by the preloaded bolt on the right end. When the exciting coil is powered on, the GMM rod overcomes the pre-compression force from the preloaded bolt to drive the output rod in the right direction.

Because the exciting coil is powered on for a long time, the resistance heat from the coil is generated; accordingly, the temperature of the GMM rod, coil bobbin, preloaded bolt, sliding block and output shaft will altogether rise, and the heat-induced displacement will appear, thereby resulting in the heat-induced displacement of GMM rod being in the right direction; however, the heat-induced displacement of the coil bobbin, preloaded bolt, sliding block and output shaft is on the left direction, which will decrease the heat-induced displacement of the GMM rod greatly. Accordingly, the output displacement precision of GMA will improve greatly as well.

By the definition of the liquid specific heat capacity, the heat flow from the coil bobbin to the liquid in the annular clearance at a period of time is as follows:

$$Q_i = t_z\Phi_{G1} \tag{16}$$

$$Q_i = mC_T\Delta T = \rho\pi(r_4^2 - r_G^2)(L_P + L_G + L_{SL} + L_O)C_T\Delta$$
$$T = \rho\pi(r_4^2 - r_G^2)L_A C_T \Delta T \tag{17}$$

where C_T is the liquid specific heat capacity, t_z is the heat transfer time, L_P, L_G, L_{SL}, L_O is the length of the preloaded bolt, GMM rod, sliding block and output shaft, respectively, and $L_A = L_P + L_G + L_{SL} + L_O$.

Based on formulas (16) and (17), the following expression can be written that the preloaded bolt temperature rise ΔT_P, the GMM rod temperature rise ΔT_G, the sliding block temperature rise ΔT_{SL} and the output shaft temperature rise ΔT_O

$$\Delta T_P = \Delta T_G = \Delta T_{SL} = \Delta T_O = \frac{t_z\Phi_{G1}}{\rho\pi(r_4^2 - r_G^2)L_A C_T} \tag{18}$$

Accordingly, the preloaded bolt temperature T_P, the GMM rod temperature T_G, the sliding block temperature T_{SL} and the output shaft temperature T_O can be written as follows

$$T_P = T_G = T_{SL} = T_O = \frac{t_z\Phi_{G1}}{\rho\pi(r_4^2 - r_G^2)L_A C_T} + T_0 \tag{19}$$

where T_0 is the start temperature of the preloaded bolt, GMM rod, sliding block and output shaft, and $T_0 = T_A$.

Based on simultaneous Eqs. (1), (2), (8), (9) and (18), the heat flow Φ_{G1} can be written as follows:

$$\Phi_{G1} = \frac{\rho\pi(r_4^2 - r_G^2)L_A C_T(R_{co} + R_h + R_A)i^2 R}{\rho\pi(r_4^2 - r_G^2)L_A C_T(R_{co} + R_h + R_A + R_{ci} + R_b + R_o) + t_z} \tag{20}$$

The temperature of the coil bobbin's inner surface is approximately equal to the liquid temperature at steady state, so the liquid temperature t_f can be written as:

$$t_f = \Delta T_G + T_0 = T_G = \frac{t_z\Phi_{G1}}{\rho\pi(r_4^2 - r_G^2)L_A C_T} + T_0 \tag{21}$$

Based on simultaneous Eqs. (12), (14) and (21), the expressions for c_1 and c_2 can be written as follows:

$$c_1 = \frac{\Phi_{G1}}{2\pi\lambda_b L_b} \tag{22}$$

$$c_2 = \left(\frac{\lambda_b}{r_4 h_{o1}} - \ln r_4\right)\frac{\Phi_{G1}}{2\pi L_b\lambda_b} + \frac{t_z\Phi_{G1}}{C_T\rho\pi(r_4^2 - r_G^2)L_A} + T_0 \tag{23}$$

So the coil bobbin temperature distribution T_b can be written as:

$$T_b = \Phi_{G1}\left[\frac{1}{2\pi L_b\lambda_b}\left(\ln\frac{r}{r_4} + \frac{\lambda_b}{r_4 h_{o1}}\right) + \frac{t_z}{C_T\rho\pi(r_4^2 - r_G^2)L_A}\right] + T_0 \tag{24}$$

Formula (24) describes the relationship between the coil bobbin's temperature distribution and the radius of coil bobbin, but the specific calculation formulas of h_o and h_A still must be identified. The dimensionless temperature gradient Nusselt number of the liquid in the coil bobbin inward can be written as follows

$$N_u = \frac{h_o l}{\lambda_o} \tag{25}$$

The Reynolds number of the fluid between the GMM rod and the coil bobbin is small, so Sieder–Tate equation can be used to calculate the average Nusselt number as follows:

$$N_u = 1.86\left(\frac{Re_f Pr_f}{l/d}\right)^{1/3}\left(\frac{\eta_f}{\eta_w}\right)^{0.14} \quad (26)$$

where Re_f is the Reynolds number under the fluid average temperature, Pr_f is Prandtl number under the fluid average temperature, η_f is dynamic viscosity under the fluid average temperature, η_w is dynamic viscosity of fluid under coil bobbin inward temperature.

Based on the simultaneous Eqs. (25) and (26), h_o can be verified. The dimensionless temperature gradient Nusselt number of the fluid on the outer cover inward surface can be written as follows

$$N_u = \frac{h_A l}{\lambda_A} \quad (27)$$

According to the free convection experimental correlation in a large space.

$$N_u = C(GrPr)_m^n \quad (28)$$

Based on simultaneous Eqs. (27) and (28), h_A can be verified. Accordingly, based on the simultaneous Eqs. (23)–(28), the temperature field distribution of the coil bobbin is completely established.

The coil bobbin heat-induced displacement can be calculated by the temperature distribution of the coil bobbin; because the temperature distribution of the coil bobbin yields an exponential distribution, the outward surface temperature of coil bobbin is higher than the other part, so the coil bobbin heat-induced displacement calculated by the outward surface temperature of the coil bobbin.

The hollow cylindrical rod with one end fixed and the other end free thermal expansion yields

$$y = \frac{2L\alpha}{r_2^2 - r_1^2}\int_{r_1}^{r_2}(T_2 - T_1)r\,dr \quad (29)$$

where L is the length of cylindrical rod, α is the linear thermal expansion coefficient of the cylindrical rod, r_1, r_2 are the inner diameter and outer diameter of hollow cylindrical rod, respectively, and T_1, T_2 are the temperature of hollow cylindrical rod before and after thermal expansion, respectively.

Based on Eqs. (18) and (29), the heat-induced displacement can be written as follows:

$$y_P = \frac{t_z \Phi_{G1}\alpha_P L_P}{\rho\pi(r_4^2 - r_G^2)L_A C_T} \quad (30)$$

$$y_G = \frac{t_z \Phi_{G1}\alpha_G L_G}{\rho\pi(r_4^2 - r_G^2)L_A C_T} \quad (31)$$

$$y_{SL} = \frac{t_z \Phi_{G1}\alpha_{SL} L_{SL}}{\rho\pi(r_4^2 - r_G^2)L_A C_T} \quad (32)$$

$$y_O = \frac{t_z \Phi_{G1}\alpha_O L_O}{\rho\pi(r_4^2 - r_G^2)L_A C_T} \quad (33)$$

$$y_{G1} = y_P + y_G + y_{SL} + y_O \quad (34)$$

where $\alpha_P, \alpha_G, \alpha_{SL}, \alpha_O$ is the thermal expansion coefficient of preloaded bolt, GMM rod, sliding block and output shaft in axial direction, respectively, and y_P, y_G, y_{SL}, y_O is the heat-induced displacement of preloaded bolt, GMM rod, sliding block and output shaft, respectively.

Based on Eqs. (24) and (29), the coil bobbin heat-induced displacement can be written as follows:

$$y_{G2} = L_b\alpha_b\Phi_{G1}\left[\left(\ln\frac{r}{r_4} + \frac{\lambda_b}{r_4 h_{o1}}\right)\frac{1}{2\pi L_b\lambda_b} + \frac{t_z}{C_T\rho\pi(r_4^2 - r_G^2)L_A}\right] \quad (35)$$

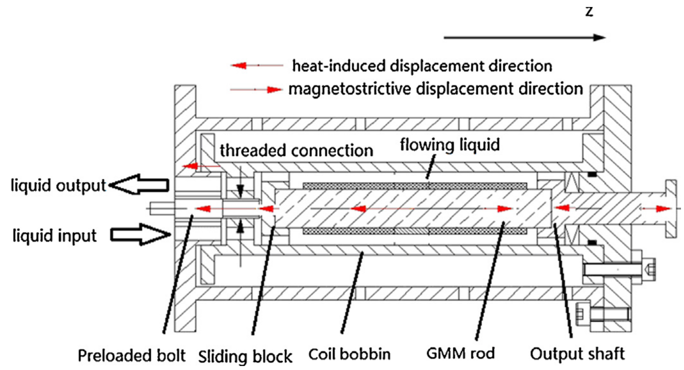

Fig. 5. Thermal compensation schematic diagram of the GMA under forced convection.

where α_b is the thermal expansion coefficient of the coil bobbin in the axial direction, and L_b is the length of the coil bobbin.

So the GMM rod heat-induced displacement with compensation of the coil bobbin can be written as follows

$$y_{G3} = y_{G1} - y_{G2} = \frac{t_z\Phi_{G1}(\alpha_P L_P + \alpha_G L_G + \alpha_{SL}L_{SL} + \alpha_O L_O)}{\rho\pi(r_4^2 - r_G^2)L_A C_T} - L_b\alpha_b\Phi_{G1}\left[\left(\ln\frac{r}{r_4} + \frac{\lambda_b}{r_4 h_{o1}}\right)\frac{1}{2\pi L_b\lambda_b} + \frac{t_z}{C_T\rho\pi(r_4^2 - r_G^2)L_A}\right] \quad (36)$$

4.3. GMA heat-induced displacement calculation model under forced convection

The thermal compensation schematic diagram of the GMA under forced convection is shown in Fig. 5, and the flowing liquid between the coil bobbin and the GMM rod replaces the motionless liquid, as shown in Fig. 4. At the steady state of heat-transfer, the heat flow Φ_{G2} generated by the coil completely transfers to the liquid in the annular clearance, which will prompt the liquid in the annular clearance to heat up.

As Fig. 5 shows, choose the GMM rod axial direction as the z direction and the infinitesimal liquid as an analytic target; thus, the infinitesimal liquid quality dm can be written

$$dm = \rho dV = \rho\pi(r_4^2 - r_G^2)dz \quad (37)$$

At heat transfer steady state, the infinitesimal heat dQ_i from the coil to the infinitesimal liquid dm can be written

$$dQ_i = t_z\frac{\Phi_{G2}}{L_A}dz \quad (38)$$

where t_z is the time that the fluid flows from the inlet to position z.

At the same time, by the definition of the liquid specific heat capacity

$$dQ_i = C_T\Delta T dm \quad (39)$$

where C_T is the specific heat capacity of the liquid.

So, based on the simultaneous Eqs. (38) and (39), the infinitesimal liquid temperature rise ΔT can be written as follows

$$\Delta T = \frac{t_z\Phi_{G2}}{C_T\rho\pi(r_4^2 - r_G^2)L_A} \quad (40)$$

Assume the flow velocity of fluid of v_1 and $t_z \geq L_A/v_1$ are based on Eqs. (20) and (40), Φ_G can be rewritten under forced convection

$$\Phi_{G2} = \frac{\rho\pi(r_4^2 - r_G^2)L_A C_T(R_{co} + R_h + R_A)i^2 R}{\rho\pi(r_4^2 - r_G^2)L_A C_T(R_{co} + R_h + R_A + R_{ci} + R_b + R_o) + L_A/v_1} \quad (41)$$

Similarly, based on Eq. (41), the average temperature rise Δt_f of the liquid between the coil bobbin and GMM rod can be written as follows

$$\Delta t_f = \frac{\Phi_{G2}}{2C_T\rho\pi(r_4^2 - r_G^2)v_1} \tag{42}$$

Accordingly the relationship between the heat transfer time and the GMM rod's average temperature at steady state can be written as follows

$$T_P = T_G = T_{SL} = T_O = \Delta t_f + T_0 = \frac{\Phi_{G2}}{2C_T\rho\pi(r_4^2 - r_G^2)v_1} + T_0 \tag{43}$$

Based on the simultaneous Eqs. (12), (14) and (42), the coil bobbin temperature T_b can be written as follows:

$$T_b = \frac{\Phi_{G2}}{2\pi L_b\lambda_b}\left(\ln\frac{r}{r_4} + \frac{\lambda_b}{r_4 h_{o2}}\right) + \frac{\Phi_{G2}}{2C_T\rho\pi(r_4^2 - r_G^2)v_1} + T_0 \tag{44}$$

Based on the simultaneous Eqs. (29) and (43), the heat-induced displacement of the preloaded bolt, sliding block and output shaft can be written as follows:

$$y_P = \frac{\Phi_{G2}\alpha_P L_P}{2\rho\pi(r_4^2 - r_G^2)C_T v_1} \tag{45}$$

$$y_G = \frac{\Phi_{G2}\alpha_G L_G}{2\rho\pi(r_4^2 - r_G^2)C_T v_1} \tag{46}$$

$$y_{SL} = \frac{\Phi_{G2}\alpha_{SL} L_{SL}}{2\rho\pi(r_4^2 - r_G^2)C_T v_1} \tag{47}$$

$$y_O = \frac{\Phi_{G2}\alpha_O L_O}{2\rho\pi(r_4^2 - r_G^2)C_T v_1} \tag{48}$$

$$y_{G1} = y_P + y_G + y_{SL} + y_O \tag{49}$$

Based on the simultaneous Eqs. (29) and (44), the coil bobbin heat-induced displacement can be written as follows:

$$y_{G2} = L_b\alpha_b\Phi_{G2}\left[\frac{1}{2\pi L_b\lambda_b}\left(\ln\frac{r}{r_4} + \frac{\lambda_b}{r_4 h_{o2}}\right) + \frac{1}{2C_T\rho\pi(r_4^2 - r_G^2)v_1}\right] \tag{50}$$

So the GMM rod heat-induced displacement with compensation of the coil bobbin can be written as follows:

$$y_{G3} = y_{G1} - y_{G2} = \frac{\Phi_{G2}(\alpha_P L_P + \alpha_G L_G + \alpha_{SL} L_{SL} + \alpha_O L_O)}{2C_T\rho\pi(r_4^2 - r_G^2)v_1} - L_b\alpha_b\Phi_{G2}\left[\frac{1}{2\pi L_b\lambda_b}\left(\ln\frac{r}{r_4} + \frac{\lambda_b}{r_4 h_{o2}}\right) + \frac{1}{2C_T\rho\pi(r_4^2 - r_G^2)v_1}\right] \tag{51}$$

Table 1
Relevant structure parameters and physical parameters for a GMA.

Name	Unit	Symbol	Value
GMM rod radius	mm	r_G	6
GMM rod length	mm	L_G	80
Coil bobbin length	mm	L_b	116
Preloaded bolt length	mm	L_P	32
Sliding block length	mm	L_{SL}	4
Output shaft length	mm	L_O	8
Cover outward radius	mm	r_1	28.5
Coil outward radius	mm	r_2	24.5
Coil bobbin outward radius	mm	r_3	15
Coil bobbin inward radius	mm	r_4	11.5
Coil resistance	Ω	R	8
The coefficient of thermal expansion for GMM rod	10^{-6}/K	α_G	12.9
The coefficient of thermal expansion for coil bobbin	10^{-6}/K	α_b	17.6
The coefficient of thermal expansion for preloaded bolt	10^{-6}/K	α_P	12.2
The coefficient of thermal expansion for sliding block	10^{-6}/K	α_{SL}	12.2
The coefficient of thermal expansion for output shaft	10^{-6}/K	α_o	12.2
Heat conductivity coefficient of liquid	W/m K	λ_L	60.8
Thermal conductivity of coil	W/m K	λ_c	398
Thermal conductivity of coil bobbin	W/m K	λ_b	16.3
Thermal conductivity of cover	W/m K	λ_h	60
Surface coefficient of heat transfer of cover outward	W/m^2 K	h_A	16
Surface coefficient of heat transfer of coil bobbin inward	W/m^2 K	h_{o1}	300
Surface coefficient of heat transfer of coil bobbin inward	W/m^2 K	h_{o2}	800
Specific heat capacity of liquid	J/kg °C	C_T	4.2×10^3
Liquid density	kg/m^3	ρ	1.0×10^3
Ambient air temperature	°C	T_A	20
Start temperature of GMM rod	°C	T_0	20

5. Theoretical model calculation results

Based on the above-mentioned GMM rod temperature rise and heat-induced displacement model and the relevant structure parameters and physical parameters for GMA presented in Table 1, computer programs for GMA steady heat-induced displacement can be programmed in MATLAB, which can be applied to a simulation study of the GMM rod temperature rise and heat-induced displacement.

First, based on Eqs. (18), (20) and (30)–(34), the exciting coil of GMA is energized by input currents of 0.6 A, 0.8 A, 1.0 A, and 1.2 A; thus, we obtain the GMM rod temperature rise and the GMM rod heat-induced displacement simulation results shown in Fig. 6, which shows that the GMM rod temperature rise and heat-induced

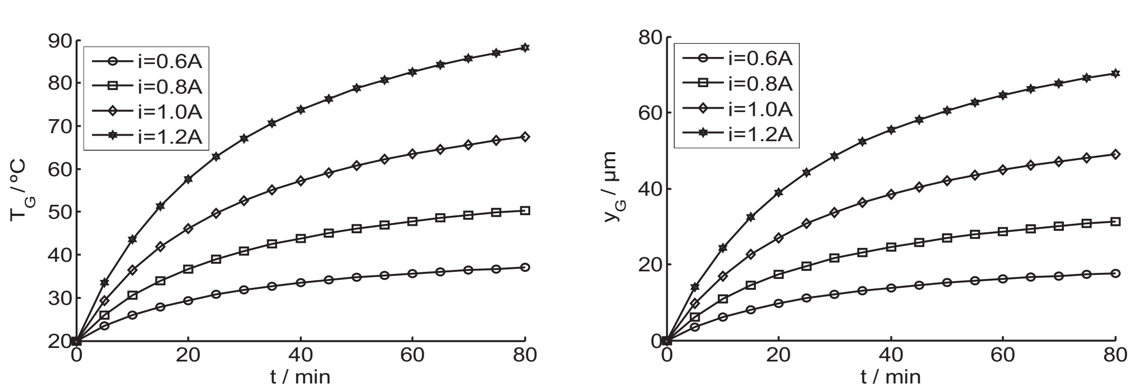

(a) (b)

Fig. 6. GMM rod temperature rise and heat-induced displacement without thermal compensation (h_A = 16).

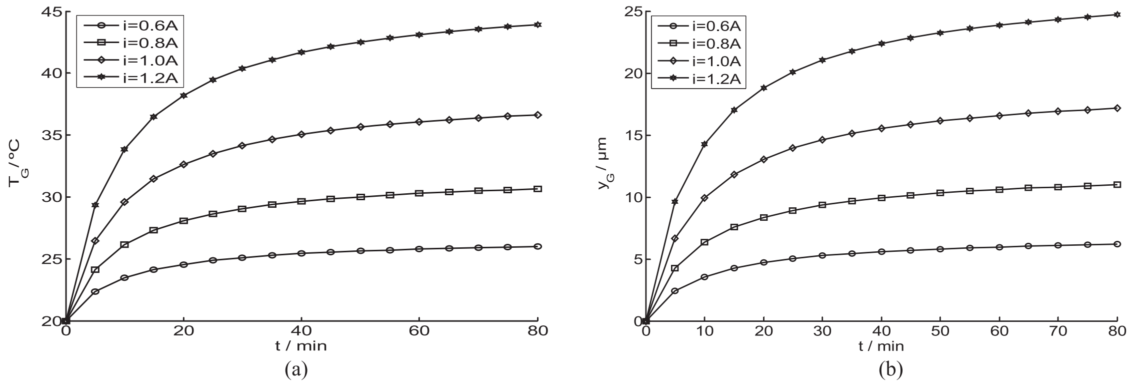

Fig. 7. GMM rod temperature rise and heat-induced displacement without thermal compensation (h_A = 56).

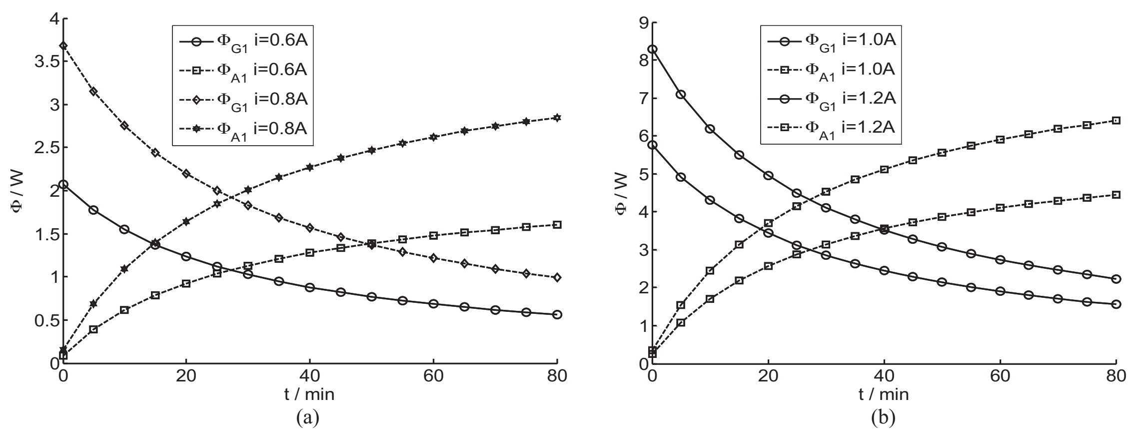

Fig. 8. The heat transfer rate of the GMA.

displacement increases with time when the exciting coil is energized for 80 min by application of a current of DC 1.0 A, the GMM rod temperature will exceed 65 °C, and the heat-induced displacement of the GMM rod will reach up to 43 μ, which is close to the displacement of the GMM rod magnetostrictive displacement. Therefore, we can draw a conclusion that GMA will not work effectively without heat-induced displacement control measures. Moreover, we perform the program by increasing the value of h_A from 16 to 56, with the simulation results shown in Fig. 7; when the exciting coil is energized for 80 min by DC 1.0 A, the GMM rod temperature will exceed 37 °C, and the heat-induced displacement of the GMM rod will reach up to 16 μ, which clearly indicates that the GMM rod temperature rise and heat-induced displacement are more sensitive to the value of h_A than to the other parameters of the GMA. Accordingly, we can decrease the GMM rod temperature rise and heat-induced displacement by increasing the value of h_A, e.g., we can cool the outer cover of the GMA using a liquid to increase the value of h_A.

Based on Eqs. (1), (2) and (20), the *heat transfer rate* Φ_{G1} conducting heat to the GMM rod through the coil bobbin and the *heat transfer rate* Φ_{A1} conducting heat to the air through the outer cover are shown in Fig. 8.

Fig. 8 shows that the *heat transfer rate* Φ_{G1} decreases with time and the *heat transfer rate* Φ_{A1} increases with time; this time

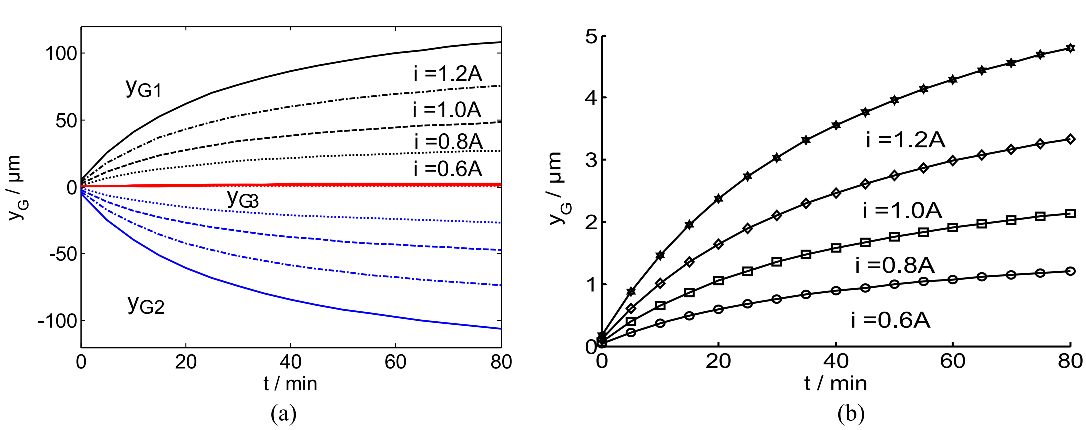

Fig. 9. GMM rod heat-induced displacement with thermal compensation under free convection.

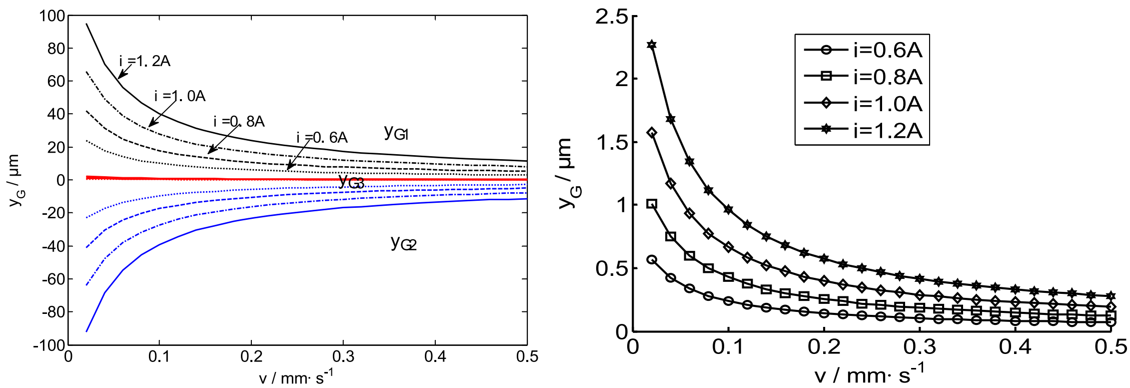

(a) (b)

Fig. 10. GMM rod heat-induced displacement with thermal compensation under forced convection.

dependence is caused by the temperature increase of the GMM rod with time, which results in the temperature potential $T_s - T_G$ decreasing with time. Accordingly, based on formula (8), the *heat transfer rate* Φ_{G1} decreases with time. Second, based on simultaneous Eqs. (20), (34)–(36), we obtain the total heat-induced displacement of the preloaded bolt, GMM rod, sliding block and output shaft y_{G1}, the coil bobbin heat-induced displacement y_{G2} and the GMM rod heat-induced displacement with thermal compensation y_{G3}, as shown in Fig. 9. The effect of thermal compensation in DC 0.6 A and DC 0.8 A is observed to be better that of DC 1.0 A and DC 1.2 A, but the result of the GMM rod heat-induced displacement with thermal compensation under free convection is unsatisfactory.

Finally, based on simultaneous Eqs. (41), (49)–(51), the input coil with DC 0.6 A, 0.8 A, 1.0 A, and 1.2 A results in the y_{G1}, y_{G2} and y_{G3} responses shown in Fig. 10; the result of the GMM rod heat-induced displacement with thermal compensation under forced convection is observed to be satisfactory.

Based on Eqs. (1), (2) and (41), the *heat transfer rate* Φ_{G2} conducting heat to the GMM rod through coil bobbin and the *heat transfer rate* Φ_{A2} conducted heat to the air through the outer cover are shown in Fig. 11.

6. Experimental investigation

The heat-transfer test system of the GMA is shown in Fig. 12. The temperature of the GMM rod is measured using a platinum resistor Pt100, the displacement of GMM rod is measured using a dial indicator (precision is 1 μm) and a laser displacement sensor (precision is 0.2 μm), a diaphragm pump supplies the liquid to cool the GMM rod, a signal generator and power amplifier supply current to the exciting coil of the GMA. In this test system, the active temperature control of the GMA is performed by the flowing liquid supplied by the diaphragm pump. The passive heat-induced displacement compensation of the GMA is achieved by the coil bobbin heat-induced movement for the up-end fixed and down-end free, which can compensate the heat-induced displacement of the GMM rod.

The test conditions and parameters are as follows: the DC input currents are 0.6 A, 0.8 A, 1.0 A, the turns per coil is 1300, the coil static resistance is 8 Ω.

The magnetostrictive displacement of the GMA is dominated by NI, the heat-induced displacement of the GMA is governed by the temperature and the thermal expansion coefficient of GMM rod, but, the magnetostrictive displacement of the GMA is also influenced by the temperature of GMM rod, therefore, firstly, a experiment have been performed to disclose the relationship that the magnetostrictive displacement y_G of GMA vs the temperature T of GMM rod in given input current value 0.6 A, 0.8 A, 1.0 A. As shown in Fig. 13, comparing with thermal displacement of GMA, the magnetostriction displacement variable quantity with the temperature is minor.

Then, the thermal displacement control experiment is performed, when the coil is energized, we immediately observe the reading of the dial indicator, with the reading indicating only magnetostrictive displacement of the GMA. After the coil was energized for a certain time period, we again observed the reading of the dial indicator, with the difference between the two observed

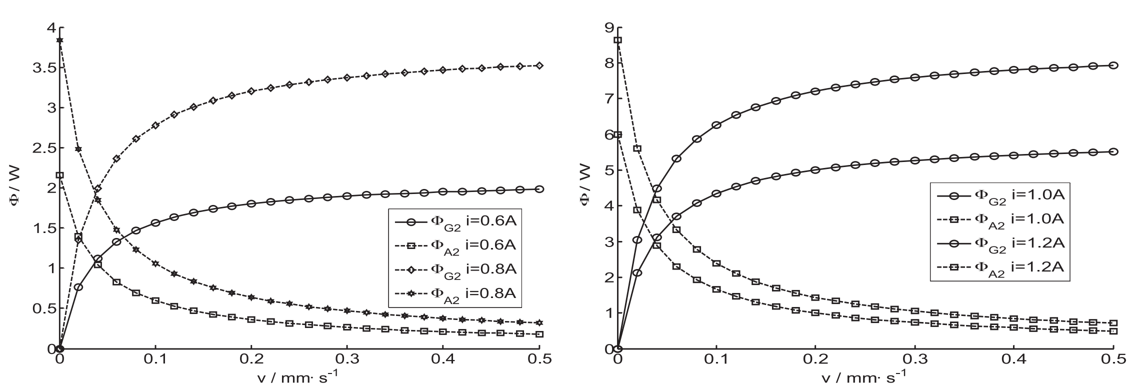

(a) (b)

Fig. 11. GMM rod heat-induced displacement with thermal compensation under forced convection.

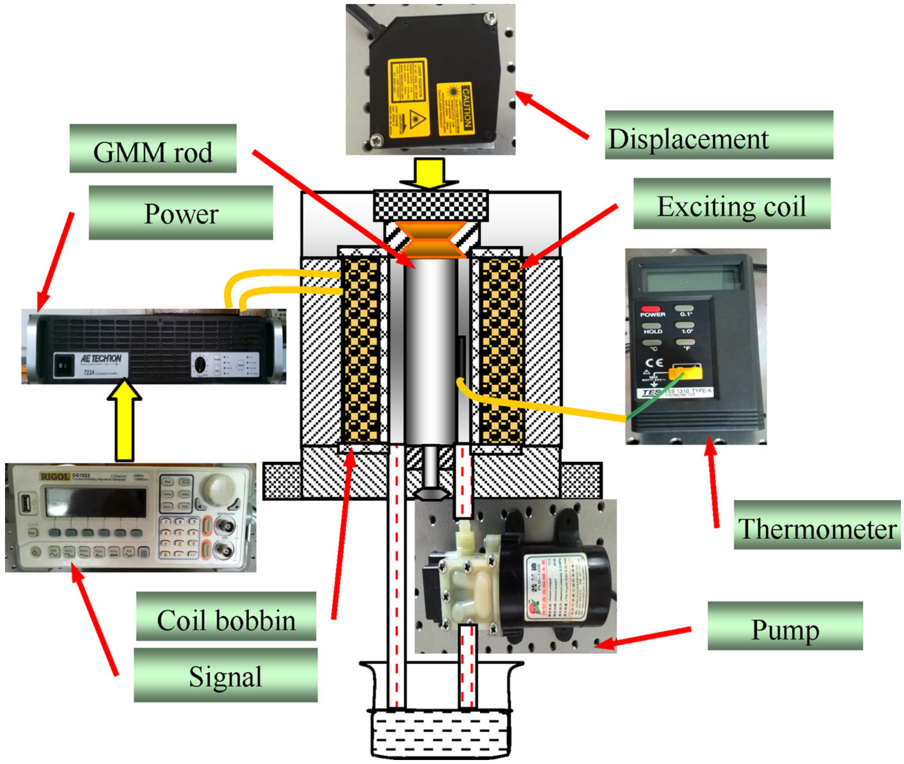

Fig. 12. Heat transfer test system of the GMA.

values being the heat-induced displacement of the GMA. The test results are shown in Figs. 14–16, which were obtained with the flow velocity of fluid $v_1 = 0.2$ mm/s. Fig. 15 is y_G vs t for GMM rod heat-induced displacement with thermal compensation under free convention, however, Fig. 16 is y_G vs t for GMM rod heat-induced displacement with thermal compensation under forced convention.

As shown in Fig. 14, that GMM rod temperature rise and the GMM rod heat-induced displacement increase continuously with time without thermal displacement control measures, and the both the GMM rod output displacement and the GMM rod temperature increase with the value of the input current. The experimental data exhibit good agreement with the model results, which verified the validity of the above-established model. As shown in Fig. 15, the GMM rod temperature continuously increases with time under free convection by thermal displacement control measures, but the GMM rod heat-induced displacement drastically decreased by the passive heat-induced displacement compensation measure under free convection. Comparing Figs. 14 and 15, the GMM rod heat-induced displacement is observed to reduce from 52 μm to 3 μm when the exciting coil of GMA is energized for 80 min.

Aiming to further improve the precision of the GMA output displacement, the test under forced convection is performed, with the experimental data and the model results shown in Fig. 16; the figure shows that the GMM rod temperature is below 35 °C and that the GMA heat-induced displacement remains within a small range under input currents of 0.6 A, 0.8 A, 1.0 A continuously operating for 80 min. The results indicate observably improved precision of the GMA output displacement under the different input current conditions. The laser displacement sensor minimum precision is 0.2 μm, as a result of that, the conclusion is that the simulation data approximate coincide with experimental data in Fig. 16(b). By above comparison, we find that the model simulation curves coincide well with experimental data, which demonstrated the validity of theoretical model presented.

Moreover, comparing Figs. 14(a), 15(a) and 16(a) with Figs. 14(b), 15(b) and 16(b), we can capture the phenomenon that experimental and theoretical simulated values of GMM rod temperature rise exhibit better agreement than that of GMM rod thermal displacement, this reason is that the coefficient of thermal expansion

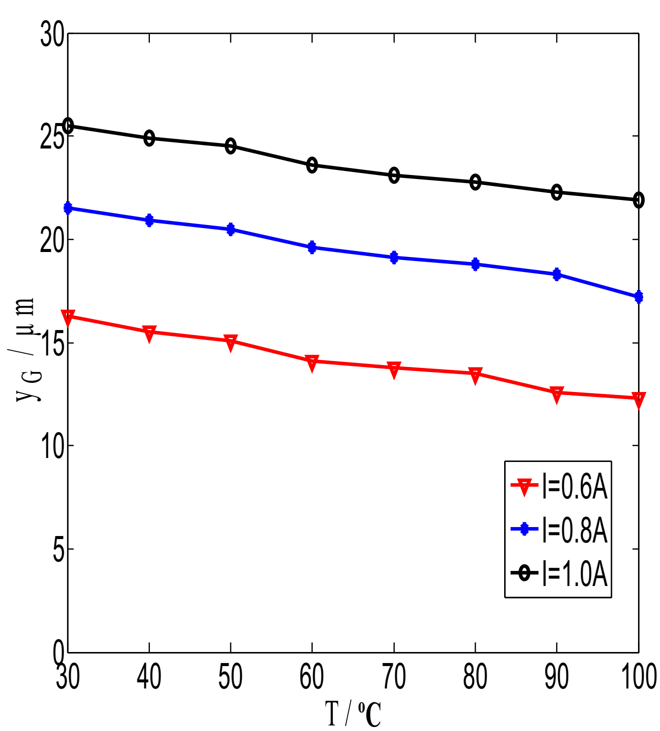

Fig. 13. Magnetostrictive displacement vs GMM rod temperature.

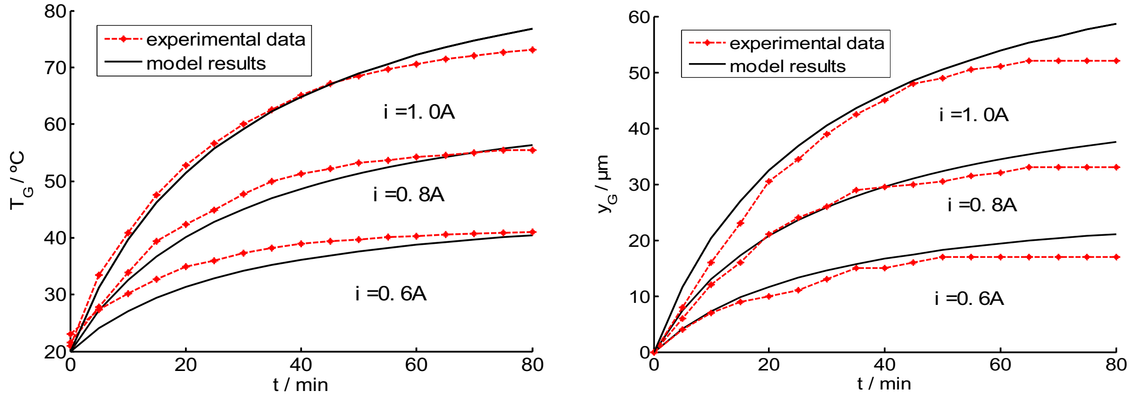

(a) (b)

Fig. 14. Test results of the GMA without thermal displacement control measures.

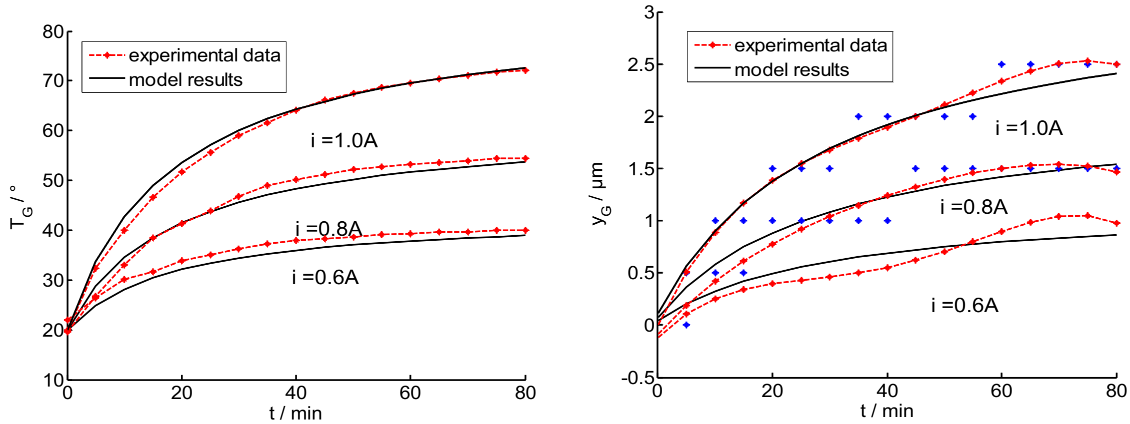

(a) (b)

Fig. 15. Test results of GMA under free convection.

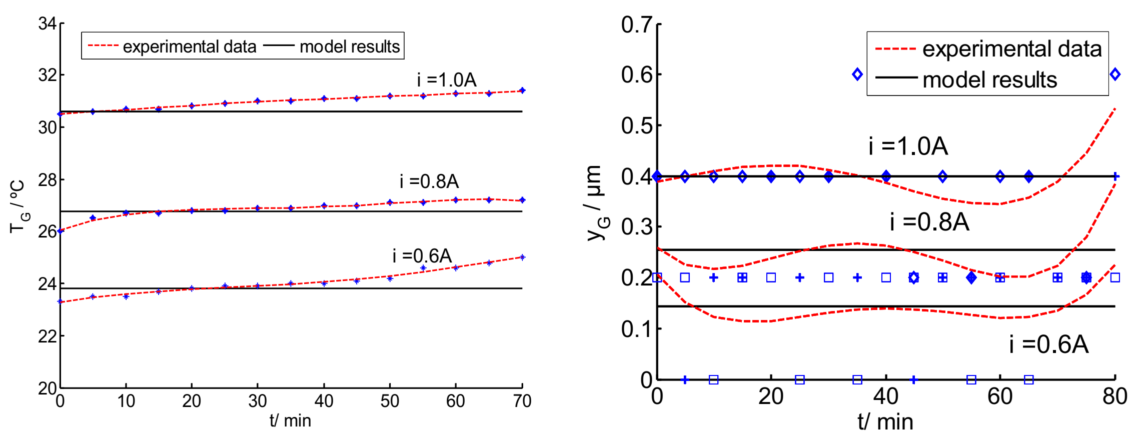

(a) (b)

Fig. 16. Test results of the GMA under forced convection.

from the components such as coil bobbin and sliding block change their values with their temperature rise.

7. Conclusion

(1) A GMA is developed with a heat-induced displacement suppression system, which consists of a temperature control module and a thermal displacement compensation module. To investigate the relationship between the GMM rod thermal deformation and the GMA parameters, we established a GMA steady-state equivalent thermal resistance model and a GMA heat-induced displacement calculation mode under free convection and forced convection.

(2) The test system for the GMA heat-induced displacement suppression system was established, and an experimental study

was performed; the results of the GMA heat-induced displacement by experimental research basically coincide with the results of the GMA heat-transfer mathematical model, which are valid only for static state.

(3) Based on the theoretical and experimental research results, for the GMA under study, the temperature is controlled to below 35 °C, and the GMA heat-induced displacement remains within a small range under 1 A input current continuously operating for 80 min, which observably improved the precision of GMA output displacement. The research results provided a basis for the application of a precise micro-displacement GMA.

Acknowledgments

This work was supported by the National Natural Science Foundation of China (grant number 51175243); the Natural Science Foundation of Jiangsu Province (BK20131359); the Aeronautical Science Foundation of China (grant number 20130652011); and the Fundamental Research Funds for the Central Universities (NS2013046).

References

[1] M. Anjanappa, J. Bi, A theoretical and experimental study of magnetostrictive mini-actuators, Smart Mater. Struct. 3 (1994) 83–91.
[2] J. Bi, A study of magnetostrictive mini-actuators (Ph.D. Dissertation), UMBC, 1998, pp. 46–52.
[3] F. Stillesjo, G. Engdahl, Z. Wei, T. Cedell, Dynamic simulation and performance study of magnetostrictive transducers for ultrasonic applications, in: Proceedings of the SPIE 3992, Smart Structures and Materials 2000: Active Materials: Behavior and Mechanics, June 14, 2000, pp. 594–602.
[4] C. Liu, Application of phase change temperature control to GMA, Combined Mach. Tool Process. Automat. Technol. 10 (2006) 50–52.
[5] K. Hiratsuka, T. Urai, Magnetic circuit design of a giant magnetostrictive actuator and application to a direct-drive servo-valve, Nippon Kikai, Gakkai Ronbunshu, B. Hen/Trans. Jpn. Soc. Mech. Eng. B 570 (1994) 479–483.
[6] M.K. Jain, S. Schmidt, C.A. Grimes, Magneto-acoustic sensors for measurement of liquid temperature, viscosity and density, Appl. Acoust. 8 (2001) 1001–1011.
[7] Y. Jia, J. Tan, Study on micro-position actuator system of giant magnetostriction materials, Chin. J. Sci. Instrum. 1 (2001) 38–41.
[8] Z. Jia, X. Yang, D. Guo, Theories and methods of designing microdisplacement actuator based on giant magnetostrictive material, J. Mech. Eng. 37 (11) (2001) 46–49.
[9] J. Xu, Y. Wu, Z. Zha, R. Ge, The design of temperature control system in giant magnetostrictive actuator, Control Detect. 10 (2007) 47–49.
[10] J.-H. Kim, H.-K. Kim, S.-B. Choi, A hybrid inchworm linear motor, Mechatronics 4 (2002) 525–542.
[11] L. Li, B. Yan, C. Zhang, Influence of frequency on characteristic of loss and temperature in giant magnetostrictive actuator, Proc. CSEE 31 (18) (2011) 124–129.
[12] L. Li, C. Zhang, B. Yan, et al., Research of a giant magnetostrictive valve with internal cooling structure, IEEE Trans. Magn. 47 (10) (2011) 2897–2900.
[13] I. Nakano, et al., Giant magnetostrictive acoustic transducer and its application to acoustic monitoring of oceans, in: International Symposium on Giant Magnetostrictive Materials and Their Applications in Japan, 1992, pp. 77–82.
[14] A.G. Olabi, A. Grunwald, Design and application of magnetostrictive materials, Mater. Des. 29 (2008) 469–483.
[15] S.C. Pradhan, Vibration suppression of FGM shells using embedded magnetostrictive layers, Int. J. Solids Struct. 42 (2005) 2465–2488.
[16] Q. Lu, C. Jing, Z. Min, et al., Integrated optimized design of GMA with double water-cooling cavums, in: International Conference on Mechanic Automation and Control Engineering (MACE), June, 2010, pp. 3562–3565.
[17] R. Angara, High Frequency High Amplitude Magnetic Field Driving System for Magnetostrictive Actuators (Ph.D. Dissertation), UMBC, 2009, pp. 64–68.
[18] X.C. Shang, E. Pan, L.P. Qin, Mathematical modeling and numerical computation for the vibration of a magnetostrictive actuator, Smart Mater. Struct. 17 (2008) 045026.
[19] L. Sun, X.J. Zheng, Numerical simulation on coupling behavior of Terfenol-D rods, Int. J. Solids Struct. 43 (2006) 1613–1623.
[20] J.P. Teter, M.H. Sendaula, J. Vranish, E.J. Crawford, Magnetostrictive linear motor development, IEEE Trans. Magn. 34 (4) (1998) 2081–2083.
[21] S. Valadkhan, K. Morris, A. Shum, A new load-dependent hysteresis model for magnetostrictive materials, Smart Mater. Struct. 19 (2010) 125003.
[22] B. Wang, S. Cao, W. Huang, Magnetostrictive Material and Devices, vol. 5, Metallurgical Industry Press, Beijing, 2008, pp. 174–186.
[23] C. Wang, F. Ding, K. Zhang, Fluid control valve based on GMA and its key techniques, Trans. Chin. Soc. Agric. Mach. 34 (5) (2003) 164–167.
[24] C. Wang, F. Ding, F. Ping, Control pressure characteristics of nozzle flapper valve based on GMA, J. Mech. Eng. 41 (5) (2005) 127–130.
[25] C. Xia, F. Ding, G. Tao, Thermal deformation compensation for giant magnetostrictive actuator, Trans. China Electrotech. Soc. 10 (5) (1999) 563–565.
[26] Y. Wu, J. Xu, Research on methods of thermal error compensating and restraining in giant magnetostrictive actuator, J. Eng. Des. 12 (4) (2005) 213–218.
[27] Y.-K. Kwak, S.-H. Kim, J.-H. Ahn, Improvement of positioning accuracy of magnetostrictive actuator by means of built-in air cooling and temperature control, Int. J. Precis. Eng. Manuf. 12 (5) (2011) 829–834.
[28] Y. Yoshio, E. Hiroshi, S. Jun, Application of giant magnetostrictive materials to positioning actuators, in: Proceeding of the IEEE/ASME International Conference on Advanced Intelligent Mechatronics, 1999, pp. 215–220.
[29] Y. Wu, Jie Xu, Research methods of thermal error compensating and restraining in giant magnetostrictive actuator, J. Eng. Des. 12 (4) (2005) 213–218.
[30] H. Zeng, G. Zeng, J. Zeng, Thermal analysis of giant magnetostrictive high power ultrasonic transducer, Proc. CSEE 31 (6) (2011) 116–120.
[31] J.J. Zheng, S.Y. Cao, H.L. Wang, W.W. Huang, Hybrid genetic algorithms for parameter identification of a hysteresis model of magnetostrictive actuators, Neurocomputing 70 (2007) 749–761.
[32] H.M. Zhou, X.J. Zheng, Y.H. Zhou, Active vibration control of nonlinear giant magnetostrictive actuators, Smart Mater. Struct. 15 (2006) 792–798.

Biographies

Yuchuan Zhu, Associate Professor, School of Mechanical and Electrical Engineering. Nanjing University of Aeronautics & Astronautics (NUAA), Nanjing 210016, P. R. China. Yuchuan Zhu was born in Huainan, China, in 1974. He received his M.S. degrees from Anhui University Science and Technology and Ph.D degree from Nanjing University of Science and Technology, respectively, all in mechanical engineering. His research area involves smart material and structure technology and fluid power transmission and control. Yuchuan Zhu was a senior member of Chinese mechanical engineering society, a member of Chinese aviation institute and Chinese aerospace institute.

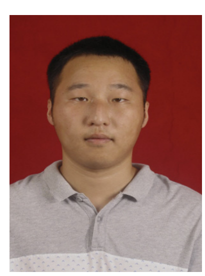

Liang Ji, Postgraduate, School of Mechanical and Electrical Engineering, Nanjing University of Aeronautics & Astronautics (NUAA), Nanjing 210016, P. R. China. His research area involves smart material and structure technology and fluid power transmission and control. Liang Ji was born in Yangzhou, China, in 1990. He received his B.S. degrees from Nanjing University of Aeronautics & Astronautics (NUAA).